

Quantitative Measures of Narrow Passages in High-dimensional Spaces and Their Efficient Sampling

G.F. Liu and J.C. Trinkle

Abstract—Narrow passages poses great challenges to many sampling-based motion planners. In problems with high-dimensional configuration spaces (C-space), narrow passages can exhibit exotic geometry which makes it hard to detect them and generate well-distributed samples on them. In this paper we first investigate the geometric model of narrow passages of a robot link through contact kinematics, which allows us to propose a rigorous definition of the narrow passages for a link, and for both open and closed chains through the kinematics of their subchains. We then present two quantitative measures, the dimension and degree of narrowness, to characterize a narrow passage. We propose the theory of topological components via deformation equivalence, which yields a coarse decomposition of the collision-free portion of the C-space (C-free). Combining the enumeration of topological components and the sampling of narrow configurations for robot links yields an efficient random sampler that produces samples in the pinching neck (called topological samples) of topological components. These samples play a key role in guiding the robot through the narrow passages. Several benchmark examples are presented that compare the performance between algorithms with and without topological samples. Animation videos and source codes are also provided which demonstrate the effectiveness of our method in solving challenging motion planning problems involving narrow passages in high-dimensional configuration spaces.

Index Terms—Path planning, cone of significant local motions, contact models, dimension and degree of narrowness, topological components, sampling of narrow passages

I. INTRODUCTION

Narrow passage problem is one of the open questions in robot motion planning. The importance of the problem was noticed since the earlier development of sampling-based motion planners [10], [20]. The challenges come mainly from the significantly smaller volume measure of narrow passages relative to the C-space itself and there are no efficient method to reliably identify them and then generate enough samples for building a well-behaved roadmap. Several indices have been proposed to characterize the narrow passages in C-space, e.g., path clearance [2], ϵ -goodness [3], expansiveness [4], and k -clearance [1]. Every measure has its own advantages and drawbacks. In high-dimensional C-spaces with complex obstacles it is difficult to calculate these indices precisely, making them not very useful in identifying the narrow passages in problems with

more than 3 degrees of freedom (DoFs). In extremal situations narrow passages could exhibit exotic geometry. For example, there exists connected components in C-space which are of measure close to 0 and everywhere narrow (e.g., the components containing configurations in Fig. 7, 9, and 12-top). This will certainly require significantly more samples in order for any of the existing probabilistic motion planners to have reasonable success rate.

Despite the difficulties of the problem, a number of progresses have been made in the past decade. Earlier progresses are mainly centered on applying different heuristics to address the challenge of narrow passage, including sampling boundaries of C-space obstacles [16], converging to medial-axis [6], [17], dilation of the free space [20], the bridge-test methods [21], manifold sampling [1], and retraction along the contact space of C-space obstacles [33]–[35]. Due to the lack of mathematical rigorously as well as the “curse of dimension” not all of these methods can be efficiently extended to high-dimensional counterparts. Techniques in [6], [16], [20], which seem quite natural in lower-dimensional spaces, is subject to explosive complexity for narrow passages in high-dimensional C-space. The bridge-test method [21] is very efficient for many high-dimensional problems, but still requires enormous bridge tests for finding good samples inside narrow passages if their codimension is greater than 1. Moreover, the desired lengths of the used bridges as well as the landscape for carrying out the bridge tests are hard to accurately estimate before sampling. Manifold-sampling approach [1] picks specific submanifolds that conforms with the narrow passage, and then generates samples on an arrangement of orthogonal submanifolds. However this method so far is only demonstrated to be successful in special examples. The retraction approach in [33]–[35] enhances the standard RRT algorithm by generating a sequence of samples on the contact space through an iterative optimization algorithm. For many narrow-passage problems, this approach often generates more samples in the entrance as well as inside the passage itself, and therefore achieves more success rate. However, this approach relies on the fact that there exists leaves on the RRT tree which are already near the narrow passage.

In recent years several new techniques have been introduced to the problem. Vonasek et al. [19] developed an iterative scaling approach to find a guiding path through narrow passages in high-dimensional C-space. Szkandera

et al. [26] proposed a modified RRT algorithm that identifies and samples the exit regions of C-space cavities, and then merges the RRT trees of the exit regions and the main RRT tree of the free space. However, when a connected component is everywhere narrow compared with the entire C-space, there will be no entrance and exiting regions with the component.

Narrow passage problem in its nature is similar but not completely same as the motion planning problem with holonomic constraints, typical examples of which are closed chains. Both problems have to address the challenges of sampling a subset of measure 0 (or close to 0) within a large ambient space. Although the domains of both problems are semi-algebraic sets, only equality constraints appear in the latter problem. When the gap of narrow passage goes to 0, the former problem converges to the latter. A number of strategies have been proposed for the resolution of equality constraints in closed chains [11]–[13], [18]. [11] approximates the holonomic constraints by semi-algebraic sets with inequalities, and the original problem turns into the sampling problem of an artificial narrow passage. Others derive samples either through the inverse kinematics (IK) of subchains [12], [13], interpolation along tangent spaces [15], or continuation across multiple local coordinate charts [22]–[24]. The C-space of closed chains itself might contain narrow passages when obstacles are introduced to their workspaces. Although narrow passages still manifests a measure 0 (or close to 0) subset on C-space submanifold, the non-Euclidean topology of the latter introduces extra complexities, not only in the decomposition of the free space into connected components [25], but also on the topology of each individual component [14]. The treatment of narrow passages for closed chains is, however, largely undeveloped.

In this paper we first investigate the near-contact model of robot links via contact kinematics, which allows us to propose a rigorous definition of narrow passages for robot links. We then derive sufficient and necessary conditions for narrow passages of open and closed chains using generalized inverse Jacobian under various categories. We propose two quantitative measures, the dimension and degree of narrowness, for identifying narrow passages and sampling along the cone of significant local motions. We define the concept of topological components based upon deformation equivalence, under which narrow passages are manifested as the pinching necks of topological components. Combing the enumeration of topological components and the sampling of narrow configurations for robot links yields an efficient algorithm for sampling the narrow passages in C-space for both open and closed chains. Our methods are demonstrated with several challenging examples including both open and closed chains.

This paper is organized as follows. In Section II we provide a rigorous definition of C-space narrow masses and two quantitative measures for their narrowness. In Section III we propose the concept of topological components and related analysis tools. In Section IV we present a new random sampling algorithm that combines narrow

configuration sampling of links and the enumeration of topological components. We present experimental results in Section V, and finally we draw conclusion in Section VI.

TABLE I
LIST OF NOTATIONS USED IN THIS PAPER

Notation	Explanation
$SE(3)$	special Euclidean group in \mathbb{R}^3
$se(3)$	Lie algebra of $SE(3)$
\mathcal{C}	C-space
c	element of \mathcal{C}
g, g_i, \hat{g}_i	element of $SE(3)$
$T_g SE(3), T_c \mathcal{C}$	Tangent space of $SE(3), \mathcal{C}$
$\mathcal{C}_{\text{obst}}$	C-Space obstacles
$\mathcal{C}_{\text{free}}$	collision-free portion of C-space
m	number of links in an open/closed chain
n	number of obstacles in workspace
$\{L_0, L_1, \dots, L_m\}$	links in an open/closed chain
$\mathcal{O} = \{\mathcal{O}_i\}$	set of obstacles in workspace
$\{p_1, \dots, p_k\}$	near-contact point set
n_i	normal vector of an object at p_i
G	grasp matrix
$\mathcal{M}, \mathcal{M}(g)$	cone of significant local motions in $se(3)$
$\mathcal{M}^*, \mathcal{M}^*(g)$	polar cone of $\mathcal{M}, \mathcal{M}(g)$
\mathcal{M}_c	cone of significant local motions in $T_c \mathcal{C}$
\mathcal{M}_c^*	polar cone of \mathcal{M}_c
$\{d_{i,0}, \dots, d_{k,0}\}$	initial gaps at near-contact point set
$\epsilon^j, \epsilon^j(c),$	narrowness metric for L_j
$\epsilon, \epsilon(g), \epsilon(c),$	narrowness metric for entire robot
δd_i	variation of gaps at near-contact point set
$\delta V, \delta V_i, \delta V_j$	twist of a rigid body in body frame
F, F_i, F_j	contact wrench in body frame
$f_i, i = 0, \dots, m$	forward kinematic map from world frame to L_i
$\{\theta_1, \dots, \theta_m\}$	joint angles of chain $\{L_0, L_1, \dots, L_m\}$
$\Theta_i = (\theta_1, \dots, \theta_i)$	joint angle vector up to L_i
g_i	configuration of L_i in world frame
Ad_g	adjoint matrix of g
\hat{g}_i	configuration of L_i w.r.t. L_0
\tilde{f}_i	forward kinematic map from L_0 to L_i
$Jf_i, J\tilde{f}_i$	Jacobian matrix of f_i, \tilde{f}_i
$R(B)$	the range space of matrix B
$N(B)$	the null space of matrix B
p_l, p_r	left and right anchors of closed chain
L^u	upper bound of arc length parameter
L^l	lower bound of arc length parameter
L	$L^u + L^l$
γ	map of chain geometry in 3-D space
γ_c	map of chain geometry at c
γ_c^{-1}	inverse of γ_c
$\gamma_{(c,\lambda)}$	deformation of γ_c by factor λ
$\text{VOL}(\gamma_c)$	volume of chain geometry
A_L	the set of links in narrow configuration

II. RIGOROUS DEFINITIONS OF NARROW PASSAGES IN C-SPACE

In this section we provide a rigorous definition of narrow passages of a rigid body in workspace, and then use it to define narrow passages in C-space of open and closed chains. Our notations are summarized in Table I.

A. Narrow passages of a rigid body

Consider first a rigid object moving among several obstacles in its workspace. Suppose it has close proximity with these obstacles, but without collision. Imagine that the rigid body is allowed to translate and rotate until some contacts are made. Then the set of near-contact points $\{p_i\}$ as well as the initial gap $d_{i,0}$ at p_i measures the narrowness of the workspace around the object.

Recall a result from multi-fingered grasping [27], [28] that an infinitesimal motion (or twist) δV of the rigid object with respect to its body frame will result in the offsets $\{\delta d_i\}$ of the set of near-contact points,

$$\begin{bmatrix} \delta d_1 \\ \vdots \\ \delta d_k \end{bmatrix} = G^T \delta V \quad (1)$$

$$G \triangleq \begin{bmatrix} n_1 & \cdots & n_k \\ p_1 \times n_1 & \cdots & p_k \times n_k \end{bmatrix}, \quad (2)$$

where $k > 0$ is the number of near-contact points and G is referred to as the grasp matrix under frictionless contacts. To avoid collision with obstacles, δd_i has to satisfy

$$d_{i,0} - \delta d_i \geq 0, \quad (3)$$

or

$$\delta d_i \leq d_{i,0} \leq \epsilon \quad (4)$$

where $\epsilon \triangleq \max_i d_{i,0} > 0$ is significantly smaller than the diameter of the object. Since a small positive offset of p_i along n_i might cause collision, any significant motion of p_i must be along $-n_i$. Therefore, the feasible set of significant local motions of the rigid body is given by

$$\mathcal{M} \triangleq \{\delta V \in se(3) \mid \delta V^T F_i \leq 0, \forall i\}. \quad (5)$$

where $F_i \triangleq [n_i^T, (p_i \times n_i)^T]^T$ are column vectors of G which are interpreted as contact wrenches. Define

$$\mathcal{M}^* \triangleq \{F \in se(3) \mid \delta V^T F \leq 0, \forall \delta V \in \mathcal{M}\}. \quad (6)$$

Fig. 1 illustrates \mathcal{M} and \mathcal{M}^* under different sets of near-contact points in 2D space.

Lemma 1. Both \mathcal{M} and \mathcal{M}^* are convex cones. $\mathcal{M}^* = \text{CONE}(G)$, the conic combination¹ of all contact wrenches. \mathcal{M} is the polar cone of \mathcal{M}^* . Moreover \mathcal{M} itself is a conic combination of a set of non-colliding twists $H = \{\delta V_j\}$, i.e., $\mathcal{M} = \text{CONE}(H)$. The decomposition of $se(3) = \mathcal{M} + \mathcal{M}^*$ is called a polar-cone decomposition.

Proof: See Appendix A. \square

We refer to \mathcal{M} as the cone of significant local motions (CSLM), and \mathcal{M}^* its polar cone.

Lemma 2. If the set of near-contact points $\{p_i\}$ is form-closure [29], i.e., the convex hull of the column vectors of G strictly contains the origin of $se(3)$, then $\mathcal{M} = \emptyset$.

¹A conic combination of a set of points is defined as a linear combination with non-negative coefficients.

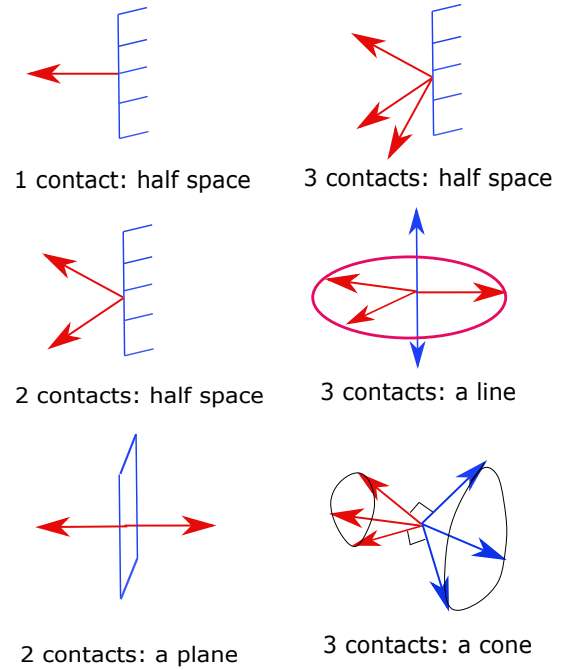


Fig. 1. Contact wrenches (in red) and the CSM (in blue) of a planar object under different sets of near-contact points

A configuration $g \in SE(3)$ is said to be *narrow* if

$$\dim \mathcal{M}(g) < 6. \quad (7)$$

In 2-D space we substitute $g \in SE(2)$ and $\dim \mathcal{M}(g) < 3$ in Eqn. (7).

Proposition 1. A configuration g of a rigid body is narrow if and only if $\mathcal{M}^*(g)$ contains a non-empty subspace.

Proof: See Appendix B. \square

The dimension of $\mathcal{M}(g)$ is referred to as the *dimension of narrowness* of g , while the *degree of narrowness* of a narrow configuration g is measured by²

$$\epsilon(g) \triangleq \max_i d_{i,0}(g). \quad (8)$$

A path $g(t) \in SE(3)$ is said to pass through a narrow passage if there exists at least one t_0 such that $g(t_0)$ is narrow. Eqn. (7) indicates that once the robot reaches $g(t_0)$, feasible samples in its neighborhood is limited to a lower dimensional subspace $\mathcal{M}(g(t_0))$.

Example 1. 1-D and 2-D narrow passages for a planar rigid body

When $\mathcal{M}(g)$, $g \in SE(2)$ is a half space or cone, g is certainly not narrow. The only possibilities are when $\mathcal{M}(g)$ is a plane or a line. Fig. 2 shows a 2-D narrow configuration under 2 near-contact points. When both near-contact points are not cusps, the narrow configuration is only 1-dimensional, see Fig. 3. If there are 3 or more non-collinear

²Notice that $\epsilon(g)$ is different from path clearance, which is often defined as $\min_i d_{i,0}$. Obviously an object with small path clearance (e.g., when it is close to an obstacle from one direction) does not mean it lies in a narrow passage.

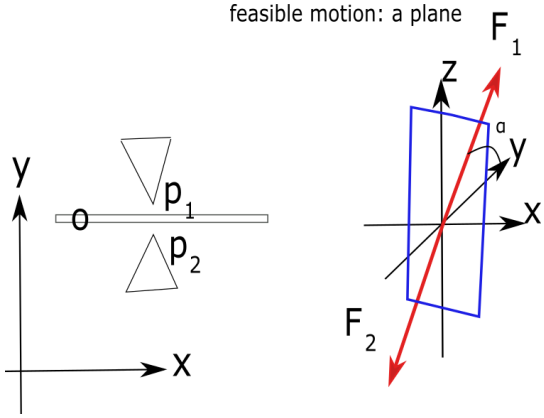


Fig. 2. An object with 2 near-contact cusp points can move along a plane (in blue) with the basis $\{x, -\sin \alpha y + \cos \alpha z\}$ of $se(2)$ (α is the angle between F_1 and y axis), i.e., translation along x -axis, and mixed translation along y -axis and rotation around z -axis. Red arrows are constraint forces.

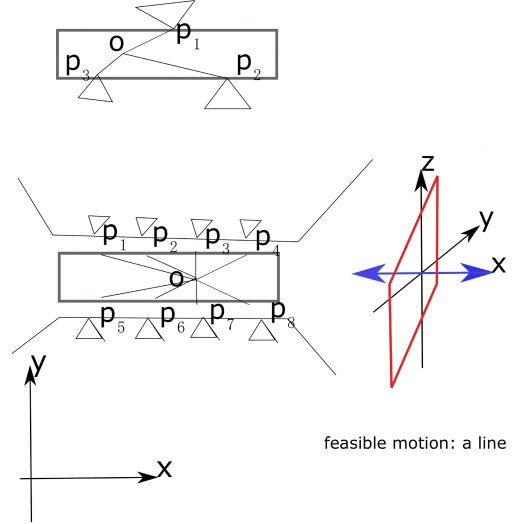


Fig. 4. An object with 3 or more non-colinear near-contact points can only translate along x -axis (in blue).

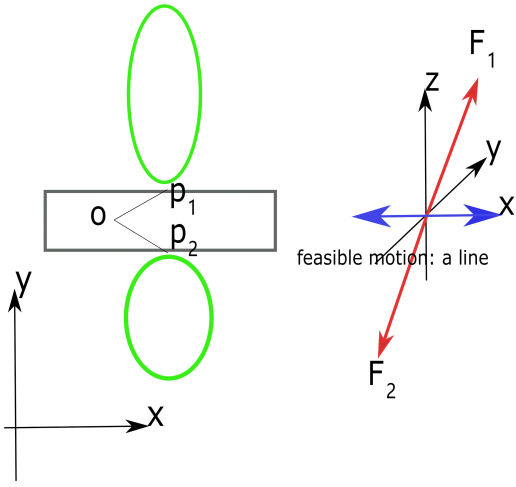


Fig. 3. An object with 2 near-contact non-cusp points can only translate along x -axis (in blue).

near-contact points, the only non-trivial narrow passage is given in Fig. 4, where the CSLM is a 1-D translation along x axis.³

Example 2. Rigid body in 3-D space

In 3-D space, the CSLM of a rigid body is generally a half-space or a cone in $se(3)$ for 1-6 near-contact points. Since we regard a narrow configuration at which the CSLM is $so(3)$ or a subspace of $so(3)$ as trivial, a few of interesting examples whose CSLM includes at least 1-D translational motion are given in Fig. 5 and 6. In Fig. 5-top the rigid body is able to translate along x-y plane (drawn in blue rectangle), and rotate around any axis by an angle within some intervals (drawn in blue and magenta arrows). In Fig. 5-bottom, the rigid body is only able to translate along x-y

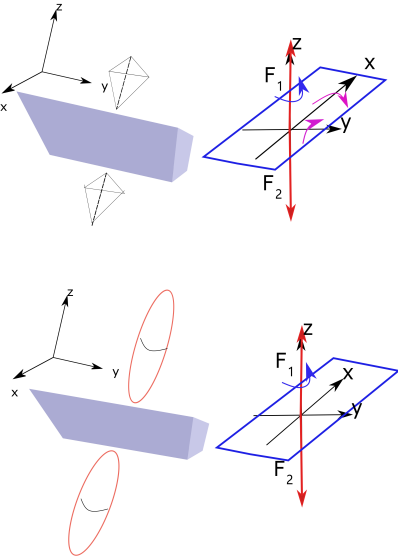


Fig. 5. A rigid body with a pair of near-contact points whose normals are in the same line. The gap between the points is assumed to be very small.

plane and rotate around z axis if the surface curvature is taken into account. Motions in the remaining DoFs cannot be significant. In Fig. 6, there are two pairs of near-contact points, the CSLM of the rigid body is the translation along x axis. .

B. Narrow passages of an open chain

An open chain is a bunch of links (L_0, L_1, \dots, L_m) connected together through joints, which are assumed here to be all revolute without loss of generality. Its C-space \mathcal{C} is simply the set of all feasible combinations of joint angles and the configuration of the base link L_0 . $\mathcal{C} = (S^1)^m$ if L_0 is a fixed base. Otherwise $\mathcal{C} = SE(3) \times (S^1)^m$, i.e., we

³If the object is circular, and moreover there are 3 or more near-contact points on its boundary whose convex hull contains the center, then the circle can only rotate around its center. However, this case is regarded as trivial here.

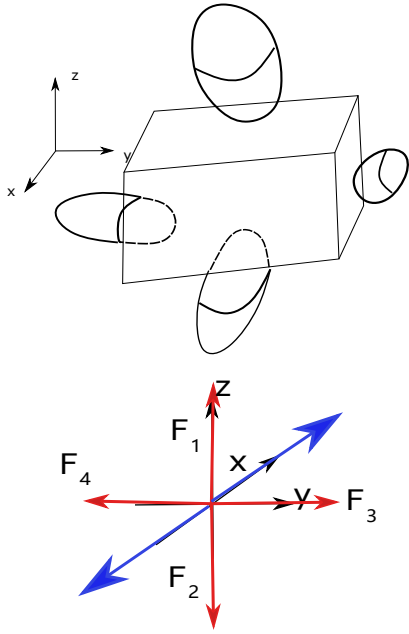


Fig. 6. An object with two pairs of near-contact points, each with their normals along the same line.

treat L_0 as a free-floating link capable of taking any pose from $SE(3)$. As L_i is a rigid body, its workspace W is a subset of $SE(3)$. W might contain narrow passages if there are obstacles in W as discussed in Subsection II-A. These narrow passages map to the corresponding narrow passages in \mathcal{C} under inverse kinematics. Recall the forward kinematic map f_i of a fragment of the chain from L_0 up to L_i is given by

$$f_0(g_0) = g_0 \quad (9)$$

$$f_i(g_0, \Theta_i) = g_0 \hat{f}_i(\Theta_i) = g_i, \quad i \geq 1 \quad (10)$$

where g_0 denotes the pose of L_0 ($g_0 = I$ if it is fixed), g_i the pose of L_i , and \hat{f}_i establishes the relation between the vector $\Theta_i = (\theta_1, \dots, \theta_i)$ of joint angles to the relative pose $\hat{g}_i = g_0^{-1}g_i$ of L_i w.r.t. L_0 . Note θ_i is the joint angle between L_{i-1} and L_i ($i \geq 1$). When $i = m$, we simply denote Θ_m as Θ . A configuration $c = (g_0, \Theta) \in \mathcal{C}$ is said to be *narrow* if there exists at least one link L_i ($0 \leq i \leq m$) such that g_i is narrow in its workspace. In fact, we might derive the space of constraint forces, and the CSLM through the Jacobian Jf_i of f_i . First $J\hat{f}_i$ of the relative forward kinematic map \hat{f}_i is given by

$$J\hat{f}_i \triangleq \hat{g}_i^{-1} \frac{\partial \hat{f}_i}{\partial \Theta_i} \quad (11)$$

if we adopt homogenous matrices representation for elements in $SE(3)$ [29]. Then Jf_i is calculated as

$$\delta V_i = g_i^{-1} \delta g_i = Ad_{\hat{g}_i^{-1}} \delta V_0 + J\hat{f}_i \delta \Theta_i \quad (12)$$

$$= \left[Ad_{\hat{g}_i^{-1}}, J\hat{f}_i \right] \begin{bmatrix} \delta V_0 \\ \delta \Theta_i \end{bmatrix} = \left[Ad_{\hat{g}_i^{-1}}, J\hat{f}_i \right] \delta c \quad (13)$$

where $\delta V_0 = g_0^{-1} \delta g_0$ is the twist of L_0 , $\delta_c = \begin{bmatrix} \delta V_0 \\ \delta \Theta_i \end{bmatrix}$, and Ad_g denotes the adjoint matrix of $g \in SE(3)$. Therefore $Jf_i = \left[Ad_{\hat{g}_i^{-1}}, J\hat{f}_i \right]$ if L_0 is free-floating, and it reduces to $J\hat{f}_i$ if L_0 is fixed.

At a narrow configuration $g_i \in SE(3)$ of L_i , its space of twists admits a polar-cone decomposition $se(3) = \mathcal{M}_i + \mathcal{M}_i^*$ with $\mathcal{M}_i^* \neq \emptyset$. This decomposition induces a corresponding polar-cone decomposition of $T_c \mathcal{C}$. Substituting $\delta V = Jf_i \delta c$ into Eqns. (5) and (6) yields

$$\mathcal{M}_c \triangleq \{ \delta c \mid \delta c^T Jf_i^T F_j \leq 0, F_j \in \mathcal{M}_i^* \} \quad (14)$$

$$\mathcal{M}_c^* = \text{CONE}(\{ Jf_i^T F_j \mid F_j \in \mathcal{M}_i^* \}), \quad (15)$$

where \mathcal{M}_c is the CSLM of the chain at $c \in \mathcal{C}$. Similar to the case of rigid body, a configuration $c \in \mathcal{C}$ is defined as narrow if the CSLM $\dim(\mathcal{M}_c) < \dim(\mathcal{C})$. Using the same technique in the proof of Proposition 1, we can prove

Proposition 2. Both \mathcal{M}_c and \mathcal{M}_c^* are convex cones. $c \in \mathcal{C}$ is narrow if and only if \mathcal{M}_c^* contains a non-empty subspace. In particular if the origin of \mathcal{C} is strictly contained in the interior of \mathcal{M}_c^* , then the entire chain is “form closure”.

Under some conditions the narrowness of g_i of L_i leads to the narrowness of c of the entire chain.

1) *Case 1: L_0 is not fixed:* In this case Jf_i is a $6 \times k$ ($k \geq 6$) matrix (assuming non-singular). As $N(Jf_i^T) = \emptyset$, any non-empty subspace $\mathcal{X} \subset \mathcal{M}_i^*$ maps to a non-empty subspace $Jf_i^T \mathcal{X} \subset \mathcal{M}_c^*$. Therefore c of the chain is narrow if and only if g_i of L_i is narrow.

2) *Case 2: L_0 is fixed, and $1 \leq i < 6$:* In this case $g_0 = I$ and Jf_i is reduced to $J\hat{f}_i$, a $6 \times i$ matrix. The chain is subject to the space of constraint forces $N(Jf_i^T)$. Denote by $\mathcal{M}_i^*/N(Jf_i^T)$ the subset of \mathcal{M}_i^* after removing the portion belonging to $N(Jf_i^T)$. Then c of the chain is narrow if and only if g_i of L_i is narrow, and moreover $\mathcal{M}_i^*/N(Jf_i^T)$ contains a non-empty subspace.

3) *Case 3: L_0 is fixed, and $i \geq 6$:* This case is same as Case 1 simply by replacing f_i (resp Jf_i) by \hat{f}_i (resp. $J\hat{f}_i$).

C. Narrow passage of a closed chain

A closed chain has both of its terminal links fixed to the ground (i.e. $L_0 = L_m$ and are fixed). Consider a given movable link L_i ($1 \leq i \leq m-1$). Without considering obstacles, its velocity space is given by $R(Jf_L) \cap R(Jf_R)$, where f_L and f_R are respectively the forward kinematics of the two fixed-base open chains (L_0, L_1, \dots, L_i) and $(L_m, L_{m-1}, \dots, L_i)$, and Jf_L and Jf_R are the Jacobian matrices of f_L and f_R , respectively. c of the chain is narrow if and only if g_i of L_i is narrow, and moreover $\mathcal{M}_i^*/(N(Jf_L^T) \cap N(Jf_R^T))$ contains a non-empty subspace.

Example 3. Narrow configurations of closed chains in 2-D and 3-D spaces

Fig. 7 illustrates a planar 9-link closed chain amoving among two polygonal obstacles. The configuration g_4 of L_4 is narrow as already discussed in Section II-A and also in Example 1, and the corresponding CSLM is 2-dimensional.

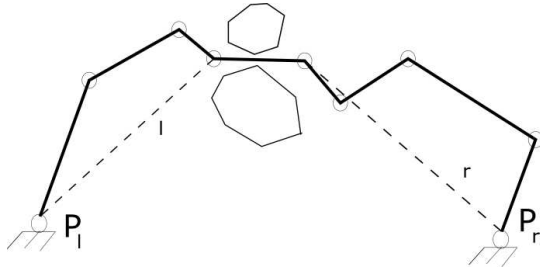


Fig. 7. Narrow configuration of a 9-link closed chain generated from a narrow configuration of link 4

It is easy to check $N(Jf_L^T) = \emptyset$ and $N(Jf_R^T) = \emptyset$. Therefore, the configuration c of this chain is also narrow. Fig. 8 gives another example where the number of links is 6, in which L_3 is narrow and $N(Jf_L^T) = \emptyset$ and $N(Jf_R^T) = \emptyset$, so does c of the entire chain. Fig. 9 shows an 8-link spatial

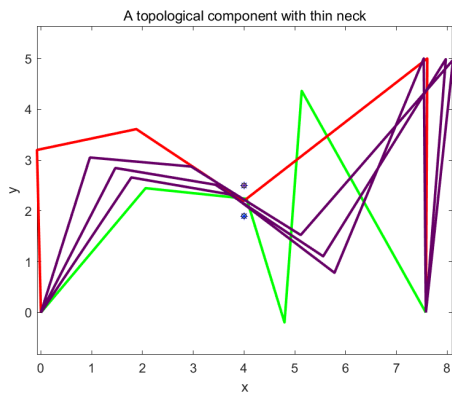


Fig. 8. Narrow configurations of a 6-bar closed chain

closed chain (assuming 0-thickness) passing through a ring-shaped obstacle of small inner-radius. As g_3 of L_3 is narrow, and moreover $N(Jf_L^T) = \emptyset$ and $N(Jf_R^T) = \emptyset$, c of the chain must be narrow.

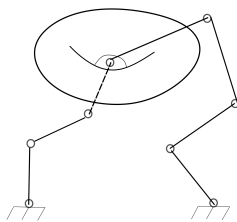


Fig. 9. A thin topological component formed by the link between a closed chain in 3-D space and a ring-shaped obstacle

D. Multiple links in narrow configurations and the degree of narrowness

When a chain has multiple links $\{L_i\}$ in narrow configurations, the CSLM of this chain will be

$$\mathcal{M}_c = \cap_i \mathcal{M}_{c,i} \quad (16)$$

where $\mathcal{M}_{c,i}$ is the CSLM of the chain when only L_i is taken into account. Each $\mathcal{M}_{c,i}$ can be calculated through its Jacobian, as given in Eqn. (14). As each $\mathcal{M}_{c,i}$ is a convex cone, \mathcal{M}_c is also a convex cone. The cone \mathcal{M}_c^* of constraint forces turns out to be

$$\mathcal{M}_c^* = \sum_i \mathcal{M}_{c,i}^*. \quad (17)$$

\mathcal{M}_c^* is a convex cone as the sum of any pair of convex cones is a convex cone. Proposition 2 also applies to the case that multiple links in a chain are in narrow configurations.

Let $\epsilon^j(c)$ be the degree of narrowness for L_j as given in Eqn. (8), then

$$\epsilon(c) = \min_j \epsilon^j(c) \quad (18)$$

provides a measure for the degree of narrowness of the entire chain. As $\epsilon^j(c)$ relies on the identification of near-contact points of L_j , it only makes sense when Link j at c is in a narrow configuration. To extend $\epsilon(c)$ to an arbitrary configuration c , we replace Eqn. (8) by

$$\epsilon^j(c) = \min_i d(L_j, \{V_i, E_i\}) \quad (19)$$

where $\{V_i, E_i\}$ is a pair of vertex and face with narrow gap (so called narrow vertex-face pair in 3D case or vertex-edge pair in 2D case), each coming from a polyhedral obstacle (or a polyhedral approximation of an arbitrary obstacle). $d(L_j, \{V_i, E_i\})$ is the maximal gap between L_j and $\{V_i, E_i\}$. When L_j possesses simple geometries, d can be effectively computed, as introduced in Subsection V-B. The algorithm for searching narrow vertex-face pairs are given in Algorithm 1.

III. TOPOLOGICAL COMPONENTS OF C-FREE

In this section, we propose the concept *topological components* for open and closed chains which allows us to generate a coarse decomposition of $\mathcal{C}_{\text{free}}$ without a priori roadmap.

A. Topological components of open and closed chains

Without loss of generality an open or closed chain can be represented as a map

$$\gamma : \mathcal{C} \times [-L^l, L^u] \rightarrow \mathbb{R}^3 \times \mathbb{R}^2, (c, s) \rightarrow (X(c, s), \Omega(s)) \quad (20)$$

where $X(c, s) \in \mathbb{R}^3$ gives the coordinates, as a function of the arclength parameter s , of every point on the 1-D backbone of the chain at configuration c , L^l and L^u are the lower and upper bounds of s , $L = L^l + L^u$ is the length of X , and $\Omega(s) \subset \mathbb{R}^2$ is a closed domain representing the cross-section of the chain at $X(c, s)$ which only depends on s . Given $c \in \mathcal{C}$, we define

$$\gamma_c : [-L^l, L^u] \rightarrow \mathbb{R}^3 \times \mathbb{R}^2, s \rightarrow \gamma(c, s), \quad (21)$$

which precisely represents the chain at configuration c . Let $\text{VOL}(\gamma_c)$ be the volume occupied by the chain, which is essentially given by integrating the area of $\Omega(s)$ along $X(c, s)$.

1) *Open chain:* Consider the following deformation along the backbone (or simply called deformation)

$$\gamma_{(c,\lambda)} : \left[-\frac{L^l}{\lambda}, \frac{L^u}{\lambda}\right] \rightarrow \mathbb{R}^3 \times \mathbb{R}^2, s \rightarrow \gamma(c, \lambda s), \quad (22)$$

where λ is referred to as the deformation scale. It is not difficult to check that $\gamma_{(c,1)} = \gamma_c$. Moreover the volume of $\gamma_c(c, \lambda)$ converges to 0 as $\lambda \rightarrow \infty$.

Lemma 3. *The volume of a chain after deformation satisfies $\text{VOL}(\gamma_{(c,\lambda)}) = \frac{1}{\lambda} \text{VOL}(\gamma_c) = \frac{1}{\lambda} \text{VOL}(\gamma_{(c,1)})$.*

Proof: See Appendix C. \square

Notice that when $\lambda < 1$, $\text{VOL}(\gamma_{(c,\lambda)}) > \text{VOL}(\gamma_c)$, and so $\gamma_{(c,\lambda)}$ can be regarded as an extension of γ_c . Conversely $\gamma_{(c,\lambda)}$ is a retraction of γ_c when $\lambda > 1$. c is said to be *deformable* if $\exists 0 < \lambda_0 \leq 1$ such that $\text{VOL}(\gamma_{(c,\lambda)})$ has no intersection with obstacles and itself $\forall \lambda \in [\lambda_0, \lambda_{\max}]$. Here λ_{\max} is the limit so that the length of the backbone $\frac{L}{\lambda}$ be greater than the maximal radius of $\Omega(s)$ among all cross-sections.

If $c \in \mathcal{C}_{\text{free}}$ is not deformable, we might decompose the entire chain into several subchains (i.e., divide $[-L^l, L^u]$ into several intervals), each deformable within its corresponding interval. It is always possible to choose the scales for these subchains so that they still constitute a complete chain without any gaps after performing deformations upon each individual subchain.

$\mathcal{C}_{\text{free}}$ can now be decomposed into components based upon the equivalence relation with respect to the set of deformable subchains. These components are referred to as *topological components*. Two configurations $c_1, c_2 \in \mathcal{C}_{\text{free}}$ are said to be in the same *topological component* if they can be broken into the same number of deformable subchains, and moreover, there exists a motion $c(t)$ between c_1 and c_2 that moves each subchain after deformation to their desired configurations without colliding with obstacles and breaking the interconnection between consecutive deformed subchains (as represented by interconnecting strings in the bottom of Fig. 11). The following Lemma states the relationship between topological components and the actual connected components of $\mathcal{C}_{\text{free}}$.

Lemma 4. *If $c_1, c_2 \in \mathcal{C}_{\text{free}}$ lie in two different topological components, they must belong to different connected components of $\mathcal{C}_{\text{free}}$.*

Example 4. Open chains with and without fixed base

In Fig. 10, two configurations c_1 and c_2 of an 4-DoF free-floating open chain are given. Both of them are deformable. It is quite simple to verify that c_1 and c_2 for the mini-chain after deformation over a given $\lambda > 1$ are connected.

Fig. 11 shows three configurations of a 9-DoF free-floating open chain. The two configurations drawn as black

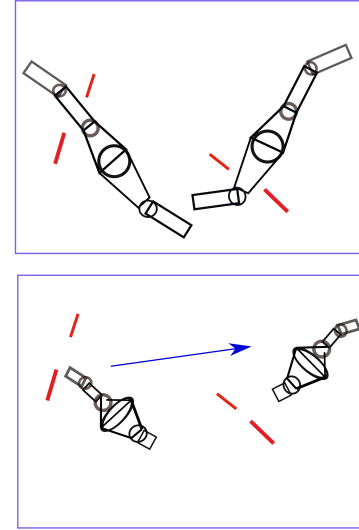


Fig. 10. Two deformable configurations of an open chain with free-floating base

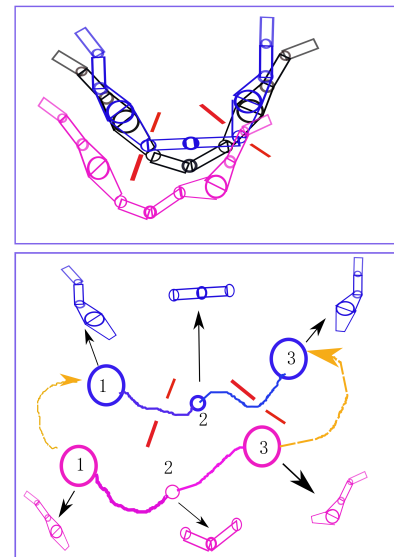


Fig. 11. Top: Three configurations of an open chain with floating base. Configurations drawn as black and blue are connected. The configuration in purple and the other two are not connected; Bottom: The chain is broken into three deformable subchains, illustrated as three balls with different radii interconnected with unbreakable string.

(c_1) and blue (c_2) are not deformable. But they are in the same connected component. The configuration drawn as purple (c_3) is deformable, however it is not in the same component as the previous two configurations. This latter result can be deduced through a topological argument. We break the chain into three deformable subchains as shown in the bottom of Fig. 11. We represent the first and last subchain as a large ball to indicate that they can not pass the two narrow passages and the entire chain at c_1 and c_2 is not deformable from either terminal of the

chain. The middle subchain is represented as a small ball because it can pass through both narrow passages. For every possible motions $c(t)$ (shown as yellow arrows) that moves the two large balls (i.e. the first and last subchains) from their corresponding configurations at c_3 to those at c_2 , the backbones of γ_{c_3} and γ_{c_2} as well as the two yellow paths forms a closed curve that can not be retracted to a point due to the obstruction from the obstacles. Therefore, c_3 is not connected with c_1 and c_2 . Appendix E shows that there are totally 23 topological components for this open chain under the deformations upon the three subchains.

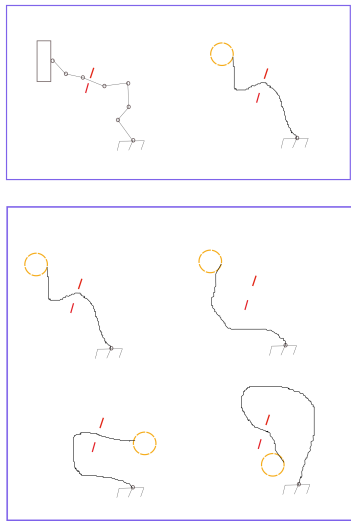


Fig. 12. Top: Undeformable configuration of an 8-DoF open chain with fixed base. It is simplified to a ball with large radius tied to the ground through a string; Bottom: Four configurations of the open chain that lie in four different topological components.

Fig. 12-top shows a non-deformable configuration of an 8-DoF open chain. This configuration can be simplified to a ball with large radius tied to the ground through a flexible string. Using the same argument as free-floating open chains, the four configurations in Fig. 12-bottom lie in four different topological components. If no two links can be fit into the narrow passages, these are the only four topological components of the chain.

2) *Closed chain:* Closed chains are certainly not deformable as a whole from either terminal. However, they can be broken into several deformable open subchains with or without fixed bases. We can directly apply the result of open chains to deduce the possible topological components for each subchain, and combine the data to obtain the topological components of the entire chain.

Proposition 3. *Given two configurations $c_1, c_2 \in \mathcal{C}_{\text{free}}$ of a closed chain. If one of its subchains lies in two different topological components at c_1, c_2 , so do c_1, c_2 for the entire chain.*

The loop-closure constraints of closed chains introduce extra topological components in addition to those from

their subchains. Recall that a closed chain of total length L at a configuration c is described by the map γ_c

$$\gamma_c : [-L^l, L^u] \rightarrow \mathbb{R}^5, s \rightarrow \gamma_c(s) = (X(c, s), \Omega(s)) \quad (23)$$

$$X(c, -L^l) = p_l, \quad X(c, L^u) = p_r. \quad (24)$$

We define the inverse γ_c^{-1} of γ_c as

$$\gamma_c^{-1} : [L^u, -L^l] \rightarrow \mathbb{R}^5, s \rightarrow \gamma_c(s). \quad (25)$$

Given two configuration $c_1, c_2 \in \mathcal{C}_{\text{free}}$ of the closed chain, define

$$\begin{cases} \gamma_{c_1}^{-1} \circ \gamma_{c_2} : [-L^l, 2L^u + L^l] \rightarrow \mathbb{R}^5, s \rightarrow \\ \left\{ \begin{array}{ll} (X(c_2, s), \Omega(s)), & -L^l \leq s \leq L^u \\ (X(c_1, 2L^u - s), \Omega(2L^u - s)) & L^u < s \leq 2L^u + L^l \end{array} \right. \end{cases}. \quad (26)$$

The backbone of $\gamma_{c_1}^{-1} \circ \gamma_{c_2}$ is a closed loop in \mathbb{R}^3 as $X(c_2, -L^l) = X(c_1, -L^l)$ and $X(c_2, L^u) = X(c_1, L^u)$.

Proposition 4. *Given $c_1, c_2 \in \mathcal{C}_{\text{free}}$, if the backbone of $\gamma_{c_1}^{-1} \circ \gamma_{c_2}$ can not be retracted to $\gamma_{c_1}^{-1} \circ \gamma_{c_1}$ without colliding with obstacles or self intersection, then they are not in the same topological component. In turn they are not in the same connected component of $\mathcal{C}_{\text{free}}$.*

Proof: See Appendix D. \square

Example 5. An example closed chain with 4 topological components

Fig. 13 shows a 12-bar planar closed chain with zero (or very small) thickness whose workspace contains 2 point obstacles. When self-intersection is not allowed, there are only 4 topological components. Configurations in these 4 components are drawn as different colors in Fig. 13.

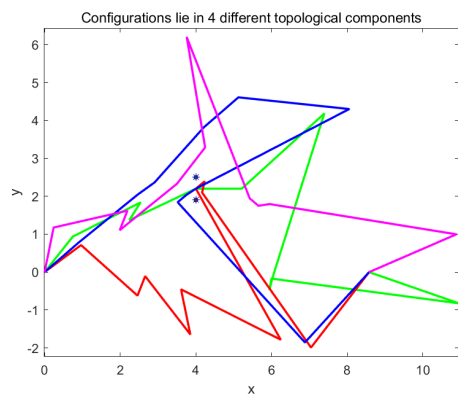


Fig. 13. A 12-bar closed chain with 2 point obstacles has 4 topological components if self-intersection is not allowed

When ignoring obstacles the only reason that prevents $\gamma_{c_2}^{-1} \circ \gamma_{c_1}$ from deforming into $\gamma_{c_1}^{-1} \circ \gamma_{c_1}$ is that the former closed curve forms a nontrivial knot.⁴

Corollary 1. *If $\gamma_{c_2}^{-1} \circ \gamma_{c_1}$ forms a nontrivial knot, then c_1, c_2 must lie two different topological components.*

⁴A knot is the embedding of a circle into \mathbb{R}^3 . A knot is nontrivial if it can not be deformed into a circle without breaking itself.

Example 6. Topological components of closed chains in 3-D space

Fig. 14-top illustrates 4 configurations of a 10-bar spatial closed chain with spherical joints. They are denoted as c_k, c_b, c_y, c_m , respectively based upon their black, blue, yellow, and magenta colors. $\gamma_{c_y}^{-1} \circ \gamma_{c_k}$ can not be deformed into $\gamma_{c_k}^{-1} \circ \gamma_{c_k}$ as will be blocked by the donut-shape obstacle. $\gamma_{c_y}^{-1} \circ \gamma_{c_m}$ can not be deformed to $\gamma_{c_y}^{-1} \circ \gamma_{c_y}$ (or $\gamma_{c_m}^{-1} \circ \gamma_{c_m}$) because it forms a nontrivial knot. c_y and c_b are not in the same topological component due to the same reason as c_y and c_k , the obstruction of the donut-shape obstacle. It is quite tricky to determine whether c_b and c_k are in the same topological component. We need the theory of linking number between two closed curves in \mathbb{R}^3 .⁵ Because c_b has different linking number around the obstacle compared with c_k , they must lie in two different topological components. As a result, these four configurations are belong to four different topological components respectively. Fig. 14-bottom illustrates two configurations (yellow and blue) of a spatial 7-bar closed chain. They are in the same topological components if the links are thin enough to pass through the gap between two cylindrical obstacles. This narrow gap manifests the existence of a narrow neck in the corresponding topological component.

IV. A NEW RANDOM SAMPLER BASED UPON CSLM AND TOPOLOGICAL COMPONENTS

In this section we propose a new random sampler that tends to sample all feasible topological components by combining a high-level subchain combinatorics and a low-level sampling algorithm of possible narrow configurations for robot links.

A. Identify the narrow passages for links

Since any workspace obstacle can be approximated by an enveloping polyhedron, possible narrow passages for a given link can be identified by finding small-gap vertex-face or face-face (in case that they are parallel) pairs, each from a different obstacle respectively. A face-face pair can always be replaced by several vertex-face pairs, as shown in Fig. 15. The searching for small-gap vertex-face pairs is achieved by the k -nn search algorithm, as given in Algorithm 1. Although different links in a given open or closed chain might have different sizes (length, width, and thickness), the search for possible narrow passages for links only needs to be carried out once in the pre-processing phase.

B. Sampling the CSLM of links at a narrow configuration

For each narrow vertex-face pair between two obstacles, the center p_c^i of link L_i can be randomly chosen from the tetrahedron formed by the vertex and the face, e.g.,

⁵Linking number is a numerical invariant that describes the linking of two closed curves in three-dimensional space. Intuitively, the linking number represents the number of times that each curve winds around the other.

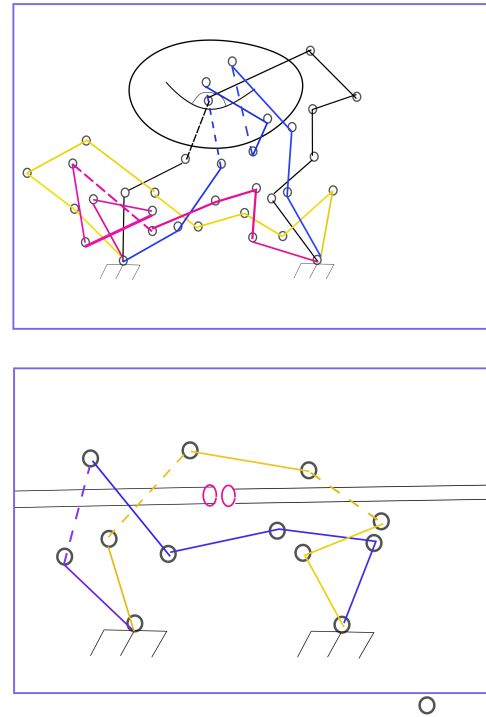


Fig. 14. Top: Four configurations of a 10-bar spatial closed chain that lie in 4 different topological components. Configurations in black and yellow are separated by a ring-shaped obstacle; Configurations in yellow and magenta form different knots; Configurations in black and blue have different linking number with the obstacle. Bottom: Two configurations of a 7-bar spatial closed chain sitting in a workspace with two cylindrical obstacles with a small gap. They are in the same connected topological component with a narrow neck.

Algorithm 1: Narrow passage identification of robot links

```

Require: polyhedron approximation
 $FV_i \triangleq \{FV_i.vertices, FV_i.faces\}$  of  $\mathcal{O}_i$ 
Ensure: find all vertex-face pairs with gaps less than a given  $\epsilon_0 > 0$ 
for Every obstacle  $\mathcal{O}_i$  do
    for Every vertex  $v_a^j$  in  $FV_i.vertices$  do
        Using  $k$ -nn search algorithm to find the closest  $k > 0$  vertices  $\{v_b^l\}$  from the approximating polyhedron of obstacles other than  $\mathcal{O}_i$ .
        Compute the distance between  $v_a^j$  and every face that contains  $v_b^l$ .
        Keep the pairs for which the distance is less than  $\epsilon_0$ .
    end for
end for

```

($A_1, \{A, B, C\}$) in Fig. 15. The feasible orientation R_i of L_i is, however, determined by its geometry. When L_i has uniform cross-sections (e.g., a cylinder or a prism), it is chosen to be parallel with the face in the pair. When L_i has irregular geometry, we randomly pick its orientations and check the collision with both obstacles that the vertex-

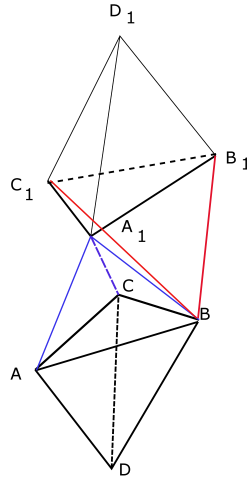


Fig. 15. Narrow face-face pair $(\{A_1, B_1, C_1\}, \{A, B, C\})$ can be replaced by $(A_1, \{A, B, C\})$, $(B_1, \{A, B, C\})$, $(C_1, \{A, B, C\})$, $(A, \{A_1, B_1, C_1\})$, $(B, \{A_1, B_1, C_1\})$, and $(C, \{A_1, B_1, C_1\})$, among which only two are drawn, $(A_1, \{A, B, C\})$ in blue and $(B, \{A_1, B_1, C_1\})$ in red.

face pair belongs to. Once we obtain a valid initial narrow configuration g_i , we perturb it along \mathcal{M}_i through a simple linear interpolation $g_i^j = g_i \circ (I + \alpha_j \delta V_j)$ with $\delta V_j \in \mathcal{M}_i$, and $\alpha_j \in \mathbb{R}$ is step size. These will generate a bunch of narrow samples in the vicinity of g_i , without considering the constraints from the chain itself.

C. Constraints from the chain

Not every random narrow configuration of L_i from Subsection IV-B has a valid IK solution. Not only the narrow configuration itself has to be reachable by its subchains (1 for an open chain, and 2 or more for a closed chain), but also the CSLM at this configuration has to have a non-empty intersection with the range space of the Jacobian of every subchain. The latter requirement is in fact can be simplified into the reachability problem of a bunch of configurations in the vicinity of a given narrow configuration, each obtained through the local perturbation along the CSLM. The final algorithm for sampling reachable narrow configurations of a given link is given in Algorithm 2.

D. Random enumeration of link indices which are in arrow configurations

Topological components of a given open or closed chain are closely related to the number of links which are at a narrow configuration, as discussed in Section III, and Example 4-6. We might randomly picks k link indices $\{i_1, \dots, i_k\}$ from a candidate set A_L of links, and associate them randomly in one-to-one correspondence with the set of narrow vertex-face pair. Consider the kinematic constraints of the chain, $A_L = \{L_0, \dots, L_m\}$ for free-floating open chains, $A_L = \{L_3, \dots, L_m\}$ for fixed-base

Algorithm 2: A random sampler of the narrow configurations of link L_i

Require: The set of narrow vertex-face pairs between obstacles, and the kinematic model of all related subchains that determines the reachable set of L_i , $0 \leq i \leq m$.

Ensure: Generate a set of random samples of L_i which are both reachable and narrow.

for Every narrow vertex-face pair **do**

- Treat the vertex and face in the pair as a pair of obstacles and compute the CSLM \mathcal{M}_i .
- Randomly pick p_c^i from the tetrahedron formed by the vertex-face pair;
- Pick a random orientation R_i for L_i which is collision-free with the pair of obstacles.
- Perform a few of small perturbations on each obtained sample $g_i = (p_c^i, R_i)$ by $g_i^j = g_i \circ (I + \alpha_j \delta V_j)$ with $V_j \in \mathcal{M}_i$, and α_j a small step size.
- If g_i is not reachable or all perturbed configurations are not reachable, discard g_i . Otherwise, keep g_i and reachable perturbations.

end for

open chains, and $A_L = \{L_3, \dots, L_{m-3}\}$ for closed chains. Moreover, $i_{k+1} - i_k \geq n_0$ ($n_0 = 3$ for 2D chains and 6 for 3D chains) to have feasible IK solutions for the subchain from L_{i_k} to $L_{i_{k+1}}$. Hence $k \leq |A_L|/n_0$, where $|A_L|$ denotes the cardinality of A_L . These k links satisfying the above constraints are referred to as an *admissible link set*. When we associate an admissible link set with a corresponding set of narrow vertex-face pairs, no two different links shall be mapped to the same narrow pair to avoid link-link collision. Combining the enumeration of admissible link set, the corresponding set of narrow vertex-face pairs, and the sampling algorithm of the narrow configurations of robot links, we obtain a new random sampler, as given in Algorithm 3, that tends to sample all possible topological components. Notice that if the cardinality of the admissible link set is 0, then we sample $\mathcal{C}_{\text{free}}$ directly with the methods in [10] for open chains, and in [12]–[15] for closed chains.

V. EXPERIMENTAL RESULTS

Algorithm 3 can be easily incorporated into the framework of both probabilistic roadmap algorithm (PRM) and the rapidly-exploring random trees (RRT), by integrating it with a local planner, a collision checking algorithm, samples from existing sampling methods without considering topological components, and a data structure (graph or tree) for recording the adjacency among samples. We call the samples from Algorithm 3 as topological samples, while those from the existing sampling methods (e.g., [11], [25], [32]) as standard samples. Similarly, we refer to the PRM or RRT algorithm without topological samples as the standard PRM (S-PRM) or RRT (S-RRT) algorithm,

Algorithm 3: A new random sampler based upon the CSLM and topological components

Require: An open or closed chain (L_0, \dots, L_m) and n obstacles $\mathcal{O}_i, i = 1, \dots, n$

Require: A set of links A_L which might be at narrow configurations

Require: A set of narrow vertex-face pairs between pairs of obstacles

Ensure: Generate N random samples that cover all possible topological components

Initialize numSample=0

while numSample < N **do**

- Randomly choose an admissible link set $\{i_1, \dots, i_k\}$ from A_L , and assign them to a corresponding set of non-repeating narrow vertex-face pairs.
- Break the chain into $k + 1$ subchains $\{i_j, \dots, i_{j+1}\}$, $j = 0, \dots, k$, $i_0 = 0$, and $i_{k+1} = m$.
- Randomly sample the narrow configurations of every all milestones in the resulting path.
- link in $\{i_1, \dots, i_k\}$ using Algorithm 2.
- Fixed the configurations of these links, call the IK of the $k + 1$ subchains to obtain the configurations of the remaining links

end while

while their counter parts with topological samples as the modified PRM (M-PRM) or RRT (M-RRT) algorithm. Our experiments have demonstrated the importance of topological samples in solving challenging narrow-passage problems for both open and closed chains, while reducing the number of standard samples.

A. Collision checking and local planner

When $\{\mathcal{O}_i\}$ are all convex, samples from the perturbation along the CSLM of a given link at a narrow configuration within a narrow vertex-face pair are certainly collision-free with the two obstacles that the pair belongs to. However, collision checking of the link with other obstacles are still required. In this paper link-obstacle and link-link collision checking are carried out through the triangulations of both links and obstacles, followed by the computation of triangle-triangle intersection.

Local planner is an important ingredient in establishing the adjacency of the roadmap graph (in the case of PRM) or the exploring tree (in the case of RRT). The local planner problem is quite different for open and closed chains. For open chains, linear interpolation in the joint space suffices to solve the problem. For closed chains, there exists no simple and continuous local planners [31]. However we may decompose \mathcal{C} into several coordinate patches [23], [25], and then construct a piecewise linear local planner by integrating paths within different coordinate patches together.

B. Degree of narrowness

In Subsection II-D, a general form of the degree of narrowness is defined for a link $\epsilon^j(c)$, and for a chain $\epsilon(c)$.

In this subsection we discuss the simple case of planar chains whose links are of rectangular shape. Given a list of narrow vertex-edge pairs $\{q_1^k, q_2^k q_3^k\}$, and also suppose that the line of symmetry of Link j is given by $p_1^j p_2^j$, we have

$$\epsilon^j(c) = \min_k \max(d(q_1^k, \overline{p_1^j p_2^j}), d(\overline{q_2^k q_3^k}, \overline{p_1^j p_2^j})) \quad (27)$$

$$\epsilon(c) = \min_j \epsilon^j(c), \quad (28)$$

where the distance function d between a point and a line segment, as well as between two line segments, can be easily computed using geometric deduction. In the experiments discussed in Subsection V-C a configuration is regarded as narrow if $\epsilon(c)$ is smaller than a given small positive constant (configurable in the code). Note that $\epsilon(c)$ can be computed for all samples generated in the sampling stage of the PRM/RRT algorithm, and also for

C. Examples

Our method was implemented in Matlab and tested for a number of challenging motion planning problems. All matlab programs were run under Windows 10 and Intel Core i7. Our software can be downloaded from <https://github.com/guanfengliu/closechain>, in which animation videos can be found for all the examples discussed below.

Example 7. A 6-bar closed chain moving among two polygonal obstacles

Fig. 16-(a) shows a 6-bar closed chain moving among two polygonal obstacles with small gap. The link length vector of this chain is $[3.2000, 2.0000, 2.5457, 4.5684, 5, 7.5815]^T$. The two polygonal obstacles are generated from two points $p_1 = [4, 1.9]^T$ and $p_2 = [4, 2.5]^T$ as

$$\mathcal{O}_1 = \text{POLY}(\{p_1 + 0.1 [\cos \beta_i, \sin \beta_i]^T\}) \quad (29)$$

$$\mathcal{O}_2 = \text{POLY}(\{p_2 + 0.1 [\cos \beta_i, \sin \beta_i]^T\}) \quad (30)$$

$$\beta_i = 2(i-1)\pi/8, \quad (31)$$

where POLY denotes a polygon formed by a sequence of vertices. The start and goal configurations are $[0.8876, -0.1414, -1.2786, 1.4988, -1.0427, 3.1416]^T$ and $[0.6889, -1.4812, 1.0114, 0.6597, -1.5765, 3.1416]^T$, respectively.

Algorithm 3 is used to generate topological samples on all of its 4 topological components, while the random loop generator of [32] is called for generating standard samples. The resulting roadmap from both sets of samples yields a collision-free path between the two configurations. The 6 path segments of this path are, respectively, shown in Fig. 16-(b), Fig. 16-(c), and Fig. 17.

Next we compare the performances of the M-PRM and the S-PRM in solving this problem. It is not difficult to see that the start and goal configurations lie in the same topological component. However, this component is everywhere narrow because for each configuration on this component, the link lying between the two point obstacles is in a narrow configuration using the same argument

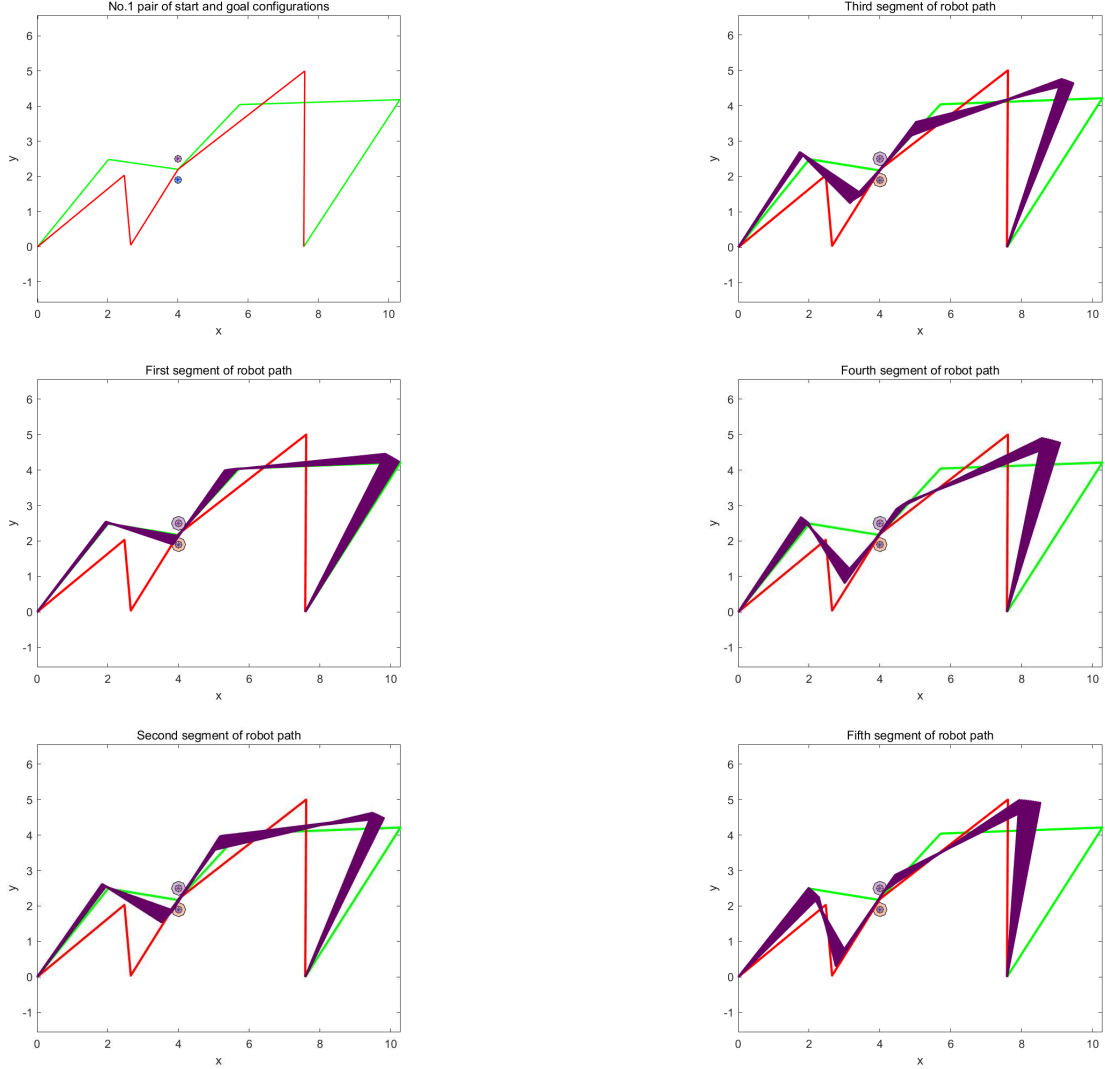


Fig. 16. (a): Start and goal configurations confined by two polygonal obstacles with small gaps; (b): First path segment; (c): Second path segment

TABLE II
PERFORMANCE COMPARISON BETWEEN THE S-PRM AND M-PRM ALGORITHMS

Algorithms	S-PRM	M-PRM
Standard samples	8000	202
Topological samples	0	1794
Components of roadmap	318	496
run time	2002.95s	217.85s
prediction	failure	success

as Example 1 and 3. Theoretically the S-PRM will take long time to generate a valid sample lying on such a component, while the M-PRM identifies and samples this topological component (as well as others) more quickly, as demonstrated by Table II.

Example 8. A 12-bar closed chain moving among two pairs of polygonal obstacles

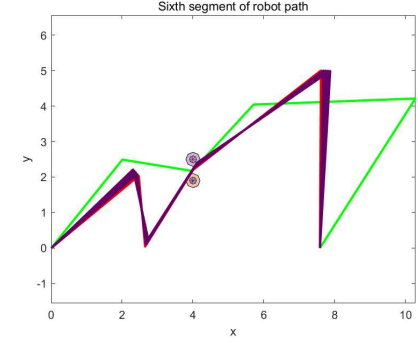


Fig. 17. (a): Third path segment; (b): Fourth path segment); (c): Fifth path segment); (d): Sixth path segment);

A 12-bar closed chain has 9 DoFs, and so can be continuously deformed between two configurations which are pinched by two pairs of polygonal obstacles, as shown in Fig. 18(a), where the link length vector is [1.2000, 2.0000, 0.5512, 1.9457, 1.2131, 2.9482, 4.5684, 0.3000, 0.3000, 5, 2.5130, 8.5815]. We apply Algorithm 3 for generating topological samples,

and similarly the random loop generator of [32] for standard samples. The resulting roadmap successfully find a path between the start configuration [$1.0631, 0.3865, 1.4542, -1.2802, -2.5472, 0.5913, -1.2102, 0.5527, 2.4609, 0.3069, 2.7463, 3.1416$] and the goal configuration [$2.2410, 0.8287, 1.0704, -0.2046, -1.6302, 0.2022, -2.2898, 1.1214, 1.6813, -0.2606, 1.1309, 3.1416$]. Again the S-PRM algorithm fails to find the right answer even after 50,000 samples, as seen in Table III.

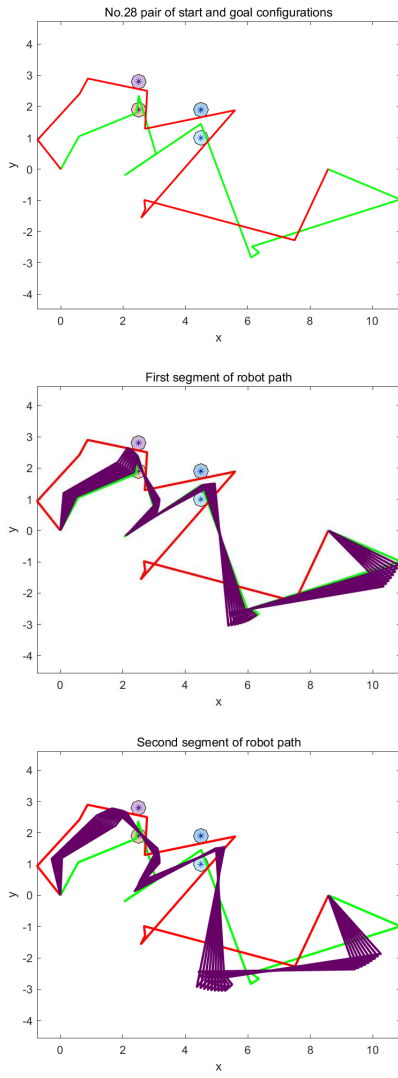


Fig. 18. (a): Start and goal configurations confined by two pairs of polygonal obstacles with small gaps; (b): First path segment; (c): Second path segment

Example 9. Path planning of a 6-DoF climbing robot on a vertical surface

Consider a 6-DoF planar robot climbing within a vertical surface with a set of holds and a number of polygonal obstacles, as shown in Fig. 20. The robot starts with an initial hold, and tries to find a sequence of holds toward a given goal hold, and the corresponding paths between any two consecutive holds in the sequence. When the

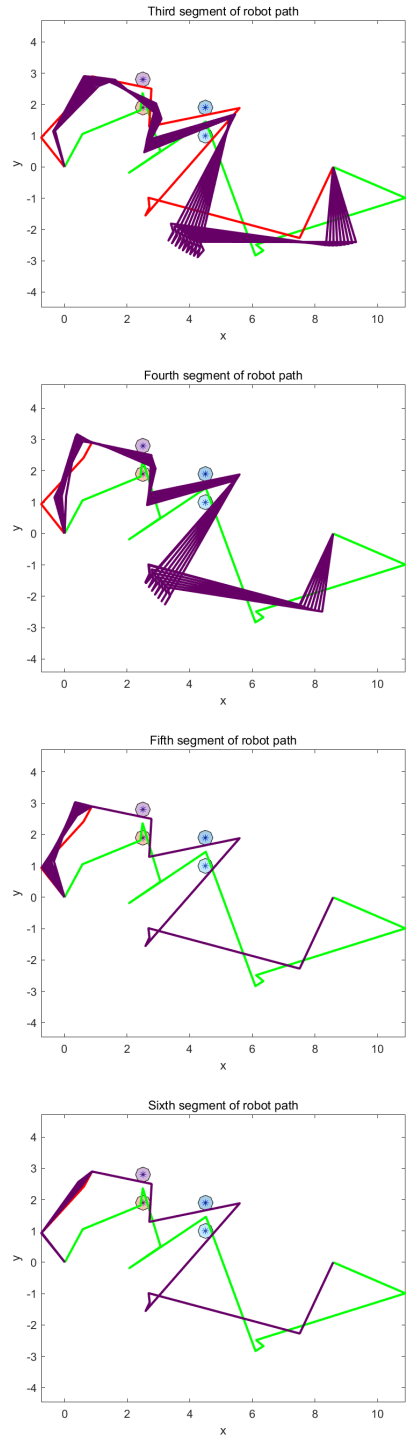


Fig. 19. (a): Third path segment; (b): Fourth path segment); (c): Fifth path segment); (d): Sixth path segment);

robot grabs the goal hold, it continues moving until a goal configuration is achieved. We call the motion between two consecutive holds and the last motion after reaching the goal hold as a phase. Within each phase, robot base, tip, and kinematic model keep constant. Upon its tip grabs a local “goal” hold, the robot gets into the next phase and a new kinematic model is used with the reversing order of

TABLE III
PERFORMANCE COMPARISON BETWEEN THE S-PRM AND M-PRM ALGORITHMS

Algorithms	S-PRM	M-PRM
Standard samples	50000	200
Topological samples	0	10048
Components of roadmap	1714	2156
Run time	8005.8s	2267s
prediction	failure	success

links.

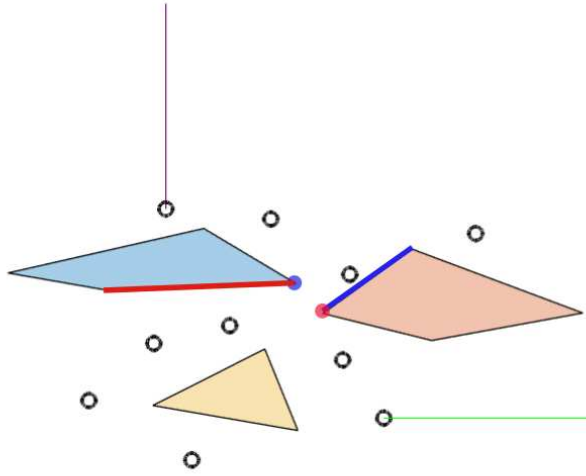


Fig. 20. A 6-DoF robot climbing in a vertical plane with 3 polygonal obstacles and 10 holds. The initial and goal configurations are respectively drawn as green and red. The pair of blue disk and edge, and the pair of red disk and edge are the two narrow vertex-edge pairs.

The setting of this problem is given as follows. The link length vector of the robot is simply set as $[1, 1, 1, 1, 1, 1]$. The workspace contains three polygonal obstacles, and 10 holds whose coordinates are respectively $[2, 1.8]^T$, $[0.8, 3.5]^T$, $[-2.5, 4.5]^T$, $[-4.7153, 3.9781]^T$, $[-6.6131, 2.3139]^T$, $[-3.6058, 0.5766]^T$, $[1.0073, 5.9927]^T$, $[-1.2993, 7.6131]^T$, $[-4.3650, 8.2051]^T$, and $[4.6861, 7.1898]^T$. Our algorithm has a preprocessing phase. It first calculates all vertex-edge pairs whose gap is less than 1.5, and yields two pairs $\{q_1^1, q_2^1 q_3^1\}$ (drawn as blue disk and edge) and $\{q_1^2, q_2^2 q_3^2\}$ (drawn as red disk and edge), both illustrated in Fig. 20. The minimal distance between the vertex and the edge of both pairs is calculated as 1.1784. 1.1784 is also the minimal gap among all obstacles. Next, it creates a hold adjacency graph that connects pairs of holds whose distances are less than the maximal reach of the robot. With the graph, it searches a list of candidate paths between the initial and goal holds, arranged in the order of total path costs (in terms of the sum of the distances between consecutive holds).

The run-time phase takes a path from the list of candidate paths, among which the shortest one is always executed first. When there is no feasible motion between any of the two consecutive holds in the sequence, the algorithm automatically switches to the next available hold sequence. The motion between a pair of holds is generated with an M-RRT algorithm, in which half of the samples are generated from purely random sampling (i.e., standard samples), and the other half from Algorithm 3 (i.e. topological samples). Our algorithm is flexible in choosing the percentage of both categories. If all samples are standard, then the algorithm goes back to the S-RRT algorithm.

We carry out both the S-RRT and M-RRT algorithms upon the same climbing problem for three different link widths (assuming all links have same link widths), 0.4, 0.6, and 0.8, respectively. The results about the computation time and the generated samples of both algorithms in each climbing phase are summarized in Table IV and V. In both tables, we denote N_i as the number of iterations for a given gait phase, N_r the number of collision-free standard sample, N_t the number of collision-free topological samples from Algorithm 3, T_s the number of leaves on the RRT tree, T_n the number of narrow samples on the tree, and T_t the number of narrow topological samples on the tree. $\frac{T_t}{T_n}$ denotes the percentage among all narrow samples on the three which are topological samples. Finally t denotes the computation time for each phase.

Both S-RRT and M-RRT can find paths when link widths are 0.4 and 0.6. However M-RRT is faster and takes less number of iterations in general in each gait phase. When link widths are 0.8, S-RRT fails to find a path at the phase $7 \rightarrow 8$ even after 1.2 million iterations, while M-RRT successfully finds a solution with much less number of iterations and computation time. The resulting path is shown in Fig. 21 and Fig. 22-(a). The narrowness for all path milestones is depicted in Fig. 22-(b). As a reference, we also show the path clearance (i.e., minimal distance from obstacles) of all milestones in Fig. 22-(c). It is as expected that path narrowness is different from path clearance. There are totally 13 narrow samples on the path which are coming from topological samples. They make it possible for the robot to navigate through the narrow passages in C-space.

We make a few remarks here to emphasize the importance of the topological samples from Algorithm 3.

Remark 1. For gait phases $2 \rightarrow 7$, $8 \rightarrow 9$, and 9 to goal, a majority of narrow samples on the RRT trees are coming from topological samples. In particular $2 \rightarrow 7$ is a phase that robot enters from an open space into a narrow passage, while $8 \rightarrow 9$ and 9 to goal can be regarded as a reverse motion of entering from open space into a narrow passage. Topological samples only occupies a small fraction of the total number of narrow samples on the tree for Phase $7 \rightarrow 8$. This is because the start configuration of this phase is already narrow, and local perturbations of this narrow configuration by steering it to any nearby standard samples

also yield narrow samples on the tree.

Remark 2. When link width is 0.8, S-RRT fails in Phase $7 \rightarrow 8$ even after 1.2 million iterations and 41922 samples. Among the 354 leaves on the tree, 309 are narrow. However, most of them falls in the second narrow vertex-edge pair (drawn as red in Fig. 20). Only a few falls in the first narrow vertex-edge pair (drawn as blue in Fig. 20), which are crucial for exiting the narrow passage. M-RRT generates narrow samples inside both narrow vertex-edge pairs, which contributed 14 among all 123 narrow samples on the tree. These 14 samples are key for successfully expanding the tree through the two narrow vertex-edge pair, as demonstrated by the fact that 13 of them were used in final path (drawn as red circles in Fig. 22-(b) and Fig. 22-(c)). Two of these key samples that falls in the first narrow vertex-edge pair are shown in Fig. 23.

Animations of the paths generated from both S-RRT and M-RRT algorithms for various link widths can be found from the github link along with source codes.

VI. CONCLUSION

This paper presents a rigorous definition of the narrow passages of a robot link based upon its near-contact kinematics. Under this model the narrowness of a link is characterized by the CSLM, and the degree of narrowness is measured by the minimal value of the largest gaps between this link and each narrow passage. We derive sufficient and necessary conditions for C-space narrow passages of both open and closed chains based upon the CSLM of robot links and the kinematics of their subchains. We then propose the tool of deformation equivalence which allows us to approximate the connected components of C-free by topological components. Combining enumeration of topological components and the sampling of the CSLM yields a new random sampler of C-space narrow passages that fuses both local and global info of C-free. Experimental results of both open and closed chains demonstrate the effectiveness of our algorithm.

ACKNOWLEDGMENT

The authors would like to thank Jim Milgram for introducing them to many of the ideas that led to the results obtained.

APPENDIX A PROOF OF LEMMA 1

First \mathcal{M} is a cone because for $\delta V_j \in \mathcal{M}$, $\alpha_j \geq 0$, and each contact wrench F_i , we have

$$\left(\sum_j \alpha_j \delta V_j \right)^T F_i = \sum_j \alpha_j \delta V_j^T F_i \leq 0,$$

So $\sum_j \alpha_j \delta V_j \in \mathcal{M}$, and \mathcal{M} is a convex cone. Similarly \mathcal{M}^* is a convex cone.

Second Eqn. (5) indicates that \mathcal{M} is a polyhedral cone, i.e., the intersections of a set of half-spaces. Therefore it must be finitely generated by a set of twists $H = \{\delta V_j\}$,

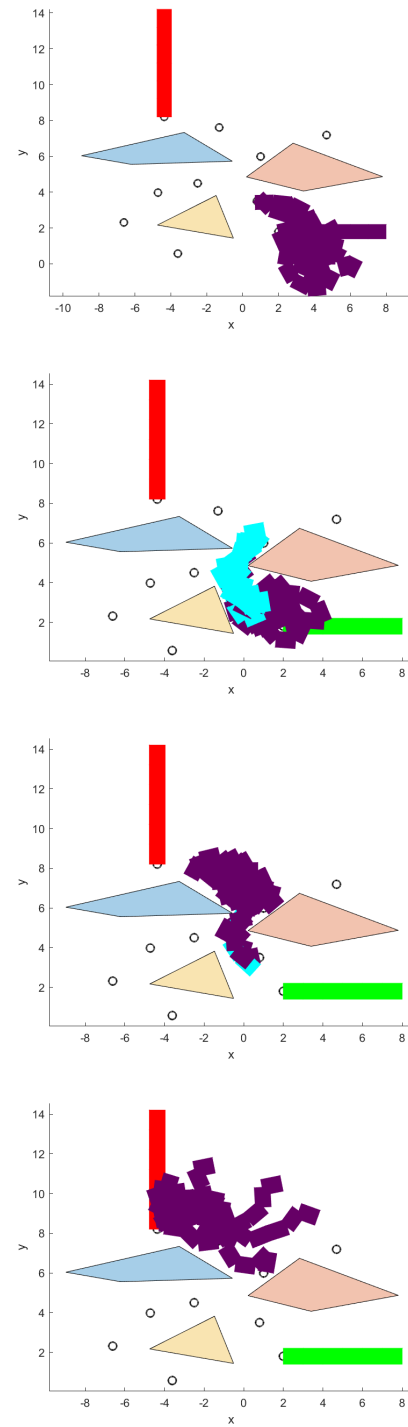


Fig. 21. Robot climbing path (link width=0.8). Narrow topological samples are shown as cyan. (a): Phase 1 → 2; (b): Phase 2 → 7; (c): Phase 7 → 8; (d): Phase 8 → 9.

i.e., $\mathcal{M} = \text{CONE}(H)$ according to the Minkowski-Weyl theorem [7], [8]. Then \mathcal{M}^* in Eqn. (6) is equivalent to

$$\mathcal{M}^* = \{F \in se(3) \mid \delta V_j^T F \leq 0, \forall j\}.$$

In other words, \mathcal{M}^* is a polyhedral cone too. Again applying the Minkowski-Weyl theorem yields that \mathcal{M}^*

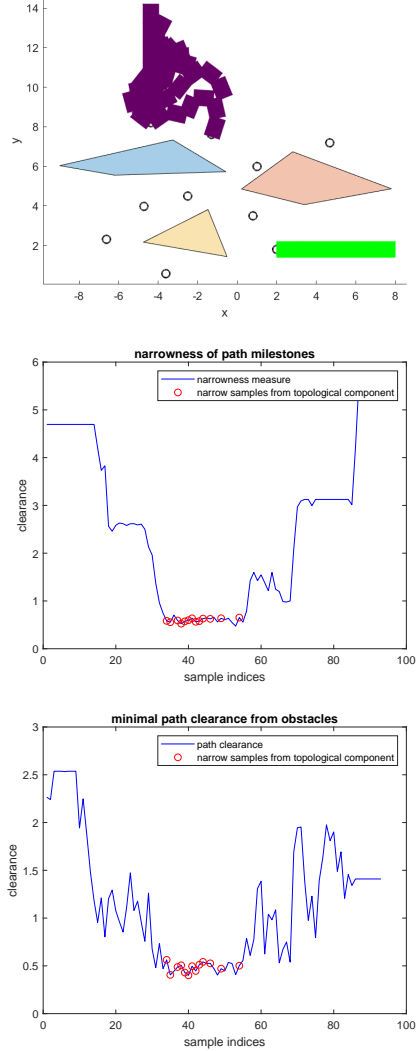


Fig. 22. (a): Phase 9 → goal; (b): Narrowness of the milestones on the robot path; (c): Path clearance of the milestones on the robot path.

must be finitely generated too. As $F_i \in \mathcal{M}^*$, it is easy to see $\mathcal{M}^* = \text{CONE}(\{F_i\})$.

APPENDIX B PROOF OF PROPOSITION 1

First, if $\mathcal{M}^*(g)$ contains a non-empty subspace \mathcal{S} , we choose $F, -F \in \mathcal{S}$. Then for any $\delta V \in \mathcal{M}(g)$, we have

$$\delta V^T F \leq 0, \quad \delta V^T (-F) \geq 0,$$

so $\delta V^T F = 0$. Therefore $\dim(\mathcal{M}(g)) < 6$ and g must be narrow.

Second, if $\dim(\mathcal{M}(g)) < 6$, then there exists a subspace \mathcal{S} which is orthogonal to $\mathcal{M}(g)$. Obviously $\mathcal{S} \subset \mathcal{M}(g)^*$, as its elements satisfy the Eqn. (6).

APPENDIX C PROOF OF LEMMA 3

Notice that the length of the chain after deformation becomes $\frac{L}{\lambda}$. Let $s' = s/\lambda$. We have $\gamma_{(c,\lambda)}(s') = \gamma(c, s)$, and

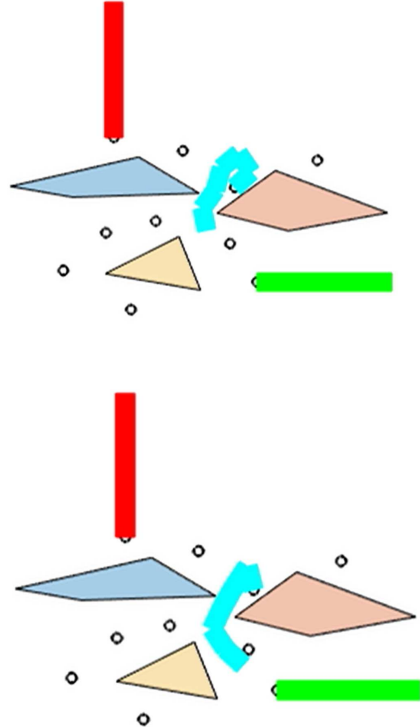


Fig. 23. Two samples (among 13) on the path which are topological samples. (a): link 5 is in narrow configuration; (b): link 3 is in narrow configuration.

so the cross-section $\Omega'(s')$ at s' of $\gamma_{(c,\lambda)}$ is exactly $\Omega(s)$ at s of γ_c . So $\int_{-\frac{L_u}{\lambda}}^{\frac{L_u}{\lambda}} \Omega'(s') ds' = \int_{-\frac{L_u}{\lambda}}^{\frac{L_u}{\lambda}} \Omega(s) ds = \int_{-L^u}^{L^u} \Omega(s) ds / \lambda$.

APPENDIX D PROOF OF PROPOSITION 4

Let $c(t), t \in [0, 1]$ be any collision-free path between c_1 and c_2 . Then $\gamma_{c(t)}^{-1} \circ \gamma_{c_2}$ is a closed curve without collision and self intersection for each t . It starts from $\gamma_{c_1}^{-1} \circ \gamma_{c_2}$ and then gradually shrinks to $\gamma_{c_1}^{-1} \circ \gamma_{c_1}$, which has volume 0. When such retraction is impossible due to the obstruction of obstacles or self intersection, then any path $c(t)$ between c_1 and c_2 is not collision-free. So they must lie in two different topological components.

APPENDIX E NUMBER OF TOPOLOGICAL COMPONENTS OF A PLANAR 9-DOF FREE-FLOATING OPEN CHAIN

The number of possible topological components for the planar free-floating open chain in Fig. 11 can be enumerated based upon the locations of ball (left or right of each hole). Assume the chain can not pass through the narrow hole twice, there are 12 possible combinations without considering the order of ball 1 and 3, as shown in Fig. 24. The final number is 23 when the order is taken into account. The last configuration in Fig. 11 doesn't change its component if ball 1 and 3 get swapped.

TABLE IV
PERFORMANCE COMPARISON BETWEEN S-RRT AND M-RRT
ALGORITHMS (LINK WIDTH = 0.4)

Phase	S-RRT	M-RRT
1 → 2	$N_i = 120000$ $N_r = 27431$ $N_t = 0$ $T_s = 20772$ $T_n = 132$ $T_t = 0$ $\frac{T_t}{T_n} = 0\%$ $tt = 270.7483s$	$N_i = 120000$ $N_r = 13604$ $N_t = 1549$ $T_s = 11052$ $T_n = 606$ $T_t = 498$ $\frac{T_t}{T_n} = 82\%$ $tt = 131.5518s$
2 → 7	$N_i = 240000$ $N_r = 25686$ $N_t = 0$ $T_s = 16208$ $T_n = 558$ $T_t = 0$ $\frac{T_t}{T_n} = 0\%$ $tt = 347.3177s$	$N_i = 120000$ $N_r = 6297$ $N_t = 3434$ $T_s = 6338$ $T_n = 873$ $T_t = 676$ $\frac{T_t}{T_n} = 77.4\%$ $tt = 113.4126s$
7 → 8	$N_i = 120000$ $N_r = 9879$ $N_t = 0$ $T_s = 902$ $T_n = 293$ $T_t = 0$ $\frac{T_t}{T_n} = 0\%$ $tt = 130.4214s$	$N_i = 120000$ $N_r = 4901$ $N_t = 383$ $T_s = 1954$ $T_n = 455$ $T_t = 111$ $\frac{T_t}{T_n} = 24.4\%$ $tt = 85.0096s$
8 → 9	$N_i = 120000$ $N_r = 20638$ $N_t = 0$ $T_s = 16093$ $T_n = 349$ $T_t = 0$ $\frac{T_t}{T_n} = 0\%$ $tt = 227.011s$	$N_i = 120000$ $N_r = 10343$ $N_t = 5186$ $T_s = 11911$ $T_n = 1208$ $T_t = 1003$ $\frac{T_t}{T_n} = 83\%$ $tt = 195.8464s$
9 → goal	$N_i = 120000$ $N_r = 20772$ $N_t = 0$ $T_s = 16267$ $T_n = 0$ $T_t = 0$ $\frac{T_t}{T_n} = 0\%$ $tt = 204.7515s$	$N_i = 120000$ $N_r = 10291$ $N_t = 17$ $T_s = 8233$ $T_n = 15$ $T_t = 14$ $\frac{T_t}{T_n} = 93.3\%$ $tt = 113.7378s$
Final path	$N_p = 108$ $N_{p,t} = 0$	$N_p = 94$ $N_{p,t} = 12$

TABLE V
PERFORMANCE COMPARISON BETWEEN S-RRT AND M-RRT
ALGORITHMS (LINK WIDTH = 0.8)

Phase	S-RRT	M-RRT
1 → 2	$N_i = 120000$ $N_r = 11557$ $N_t = 0$ $T_s = 8853$ $T_n = 9$ $T_t = 0$ $\frac{T_t}{T_n} = 0\%$ $tt = 174.1437s$	$N_i = 120000$ $N_r = 5728$ $N_t = 626$ $T_s = 4555$ $T_n = 27$ $T_t = 24$ $\frac{T_t}{T_n} = 88.9\%$ $tt = 70.6838s$
2 → 7	$N_i = 600000$ $N_r = 24059$ $N_t = 0$ $T_s = 16874$ $T_n = 46$ $T_t = 0$ $\frac{T_t}{T_n} = 0\%$ $tt = 384.8021s$	$N_i = 840000$ $N_r = 16720$ $N_t = 2969$ $T_s = 13514$ $T_n = 141$ $T_t = 116$ $\frac{T_t}{T_n} = 82.26\%$ $tt = 395.0018s$
7 → 8 (fails)	$N_i = 1200000$ $N_r = 41922$ $N_t = 0$ $T_s = 354$ $T_n = 309$ $T_t = 0$ $\frac{T_t}{T_n} = 0\%$ $tt = 520.9913s$	$N_i = 720000$ $N_r = 12526$ $N_t = 74$ $T_s = 1714$ $T_n = 123$ $T_t = 14$ $\frac{T_t}{T_n} = 11.4\%$ $tt = 288.4539s$
8 → 9		$N_i = 120000$ $N_r = 4504$ $N_t = 1267$ $T_s = 4253$ $T_n = 8$ $T_t = 8$ $\frac{T_t}{T_n} = 100\%$ $tt = 97.4197s$
9 → goal		$N_i = 120000$ $N_r = 4682$ $N_t = 3$ $T_s = 3810$ $T_n = 0$ $T_t = 0$ $\frac{T_t}{T_n} = 0\%$ $tt = 70.7142s$
Final path		$N_p = 93$ $N_{p,t} = 13$

REFERENCES

- [1] O. Salzman, M. Hemmer and D. Halperin, *On the Power of Manifold Samples in Exploring Configuration Spaces and the Dimensionality of Narrow Passages*. IEEE Transactions on Automation Science and Engineering, Vol. 12, No. 2, pp. 529-538, April, 2015
- [2] L. E. Kavraki, M. N. Kolountzakis, and J.C. Latombe, *Analysis of Probabilistic Roadmaps for Path Planning*. IEEE Transactions on Robotics, Vol. 14, No. 1, pp. 166-171, February, 1998.
- [3] L. E. Kavraki, J.-C. Latombe, R. Motwani, and P. Raghavan, *Randomized query processing in robot path planning*. J. Comput. Syst. Sci, Vol. 57, No. 1, pp. 50-60, August 1998.
- [4] D. Hsu, J. Latombe, and R. Motwani, *Path planning in expansive configuration spaces*. Int. J. Comp. Geo. and App., Vol. 4, pp. 495-512, 1999.
- [5] C. Holleman and L. E. Kavraki, *A framework for using the workspace medial axis in PRM planners*, "Proceedings 2000 ICRA. Millennium Conference". IEEE International Conference on Robotics and Automation. Symposia Proceedings (Cat. No.00CH37065), PP. 1408-1413, San Francisco, CA, USA, 2000.
- [6] M. Saha, J. Latombe, Y. Chang, Lin, and F. Prinz, *Finding narrow passages with probabilistic roadmaps: the small step retraction method*. Intelligent Robots and Systems, vol. 19, no. 3, pp. 301-319, Dec 2005.
- [7] S.P. Boyd and L. Vandenberghe, *Convex Optimization*. Cambridge University Press, ISBN 978-0-521-83378-3, 2004.
- [8] G. Ziegler, *Lectures on polytopes*, Springer-Verlag, 1997.
- [9] J. Meng, G.F. Liu, and Z.X. Li, *A Geometric Theory for Synthesis and Analysis of Sub-six DoF Parallel Manipulators*. IEEE Transactions on Robotics, Vol. 23, No. 4, PP. 625-649, 2007.
- [10] L.E. Kavraki, P. Švestka, J.C. Latombe, and M.H. Overmars,

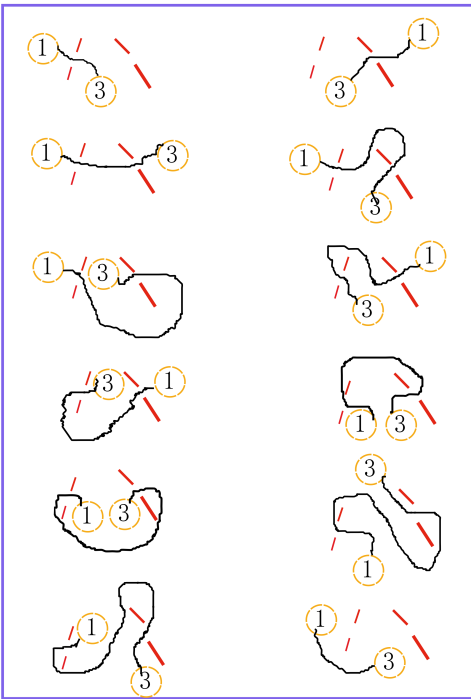


Fig. 24. 12 different combinations of two large balls interconnected with a string (representing three subchains of the planar open chain in Fig. 11).

Probabilistic Roadmaps for path planning in high-dimensional configuration space. IEEE Transactions on Robotics and Automation, 12(4):566-580, 1996.

- [11] J. Yakey, S. M. LaValle, and L. E. Kavraki, *Randomized path planning for linkages with closed kinematic chains*. IEEE Transactions on Robotics and Automation, 17(6):951–958, December 2001.
- [12] J. Cortes, *Motion planning algorithms for general closed-chain mechanisms*. Doctorat, Institut National Polytechnique, Toulouse, December 16, 2003, 160p.
- [13] L. Han and N.M. Amato, *A kinematics-based probabilistic roadmap method for closed chain systems*. in Algorithmic and Computational Robotics: New Directions, B.R. Donald, K.M. Lynch, and D. Rus, Eds. AK Peters, Wellesley, PP. 233-246, 2001.
- [14] J.C. Trinkle and R.J. Milgram, *Complete Path Planning for Closed Kinematic Chains with Spherical Joints*. International Journal of Robotics Research, 21(9):773-789, December, 2002.
- [15] Beobkyoon Kim, Terry Taewoong Um, Chansu Suh and F. C. Park, *Tangent bundle RRT: A randomized algorithm for constrained motion planning*. Robotica, 34, pp 202-225 doi:10.1017/S0263574714001234.
- [16] N. Amato, O. Bayazit, L. Dale, C. Jones, D. Vallejo, *OBPRM: An obstacle-based PRM for 3D workspaces*. in: P.K. Agarwal, L.E. Kavraki, M.T. Mason (eds.), *Robotics: The algorithmic perspective*, A.K. Peters, Natick, 1998, pp. 155-168.
- [17] C. Holleman and L.E. Kavraki, *A Framework for Using Workspace Medial Axis in PRM Planners*, Proceedings - IEEE International Conference on Robotics and Automation, PP. 1408-1413, 2000.
- [18] D. Berenson, S. Srinivasa, D. Ferguson and J. Kuffnerr, *Manipulation Planning on Constraint Manifolds*. Proceedings - IEEE International Conference on Robotics and Automation, PP. 625-632, 2009.
- [19] V. Vonasek, J. Faigl, T. Krajnik, L. Preucil, *A sampling schema for rapidly exploring random trees using a guiding path*. Proceedings of the 5th European Conference on Mobile Robots, vol. 1, pp. 201-206, 2011.

- [20] D. Hsu, L.E. Kavraki, J.C. Latombe, R. Motwani, and S. Sorkin, *On finding narrow passages with probabilistic roadmap planners*. Proceedings of the third workshop on the algorithmic foundations of robotics: the algorithmic perspective, PP. 141-153, 1998.
- [21] Zheng Sun, D. Hsu, T. Jiang, H. Kurniawati and J. H. Reif, *Narrow passage sampling for probabilistic roadmap planning*. IEEE Transactions on Robotics, vol. 21, no. 6, pp. 1105-1115, Dec. 2005.
- [22] Porta J.M., Jaillet L., *Path Planning on Manifolds Using Randomized Higher-Dimensional Continuation*. In: Hsu D., Isler V., Latombe JC., Lin M.C. (eds) Algorithmic Foundations of Robotics IX. Springer Tracts in Advanced Robotics, Vol. 68, PP. 337-353, Springer, 2010.
- [23] Jaillet L., Porta J.M., *Path Planning with Loop Closure Constraints Using an Atlas-Based RRT*. In: Christensen H., Khatib O. (eds) Robotics Research. Springer Tracts in Advanced Robotics, Vol. 100, PP. 345-362, 2017.
- [24] C. Voss, M. Moll and L.E. Kavraki. *Atlas + X: Sampling-based Planners on Constraint Manifolds*. (2017) <http://hdl.handle.net/1911/96421>.
- [25] G.F. Liu, J.C. Trinkle, Y. Yang, and S.M. Luo, *Motion Planning of Planar Closed Chains With Structural Sets*, IEEE Access, Vol. 8, PP. 117203-117217, 2020.
- [26] J. Szkandera, I. Kolingerova, M. Manak, *Narrow Passage Problem Solution for Motion Planning*. In: V. Krzhizhanovskaya et al. (eds) Computational Science - ICCS 2020. Lecture Notes in Computer Science, Vol. 12137, PP. 459-470, Springer, Cham.
- [27] A. Bicchi, *On the Closure Properties of Robotic Grasping*. International Journal of Robotics Research, Vol. 14, No. 4, PP. 319-334, 1995.
- [28] M.Y. Wang, *An optimum design for 3-D fixture synthesis in a point set domain*. IEEE Transactions on Robotics and Automation, Vol. 16, No. 6, PP. 839-846, 2000.
- [29] R.M. Murray, Z.X. Li, and S.S. Sastry, *A Mathematical Introduction to Robotic Manipulation*, CRC Press, 1994.
- [30] E.G. Gilbert, D.W. Johnson, and S.S. Keerthi. *A Fast Procedure for Computing the Distance Between Objects in Three-Dimensional Space*, IEEE Transactions on Robotics and Automation, RA(4)(1988), pp. 193-203.
- [31] M. Farber, *Topological Complexity of Motion Planning*, Discrete Comput. Geom. 29:211-221 (2003).
- [32] J. Cortes, *Motion planning algorithms for general closed-chain mechanisms*. Doctorat, Institut National Polytechnique, Toulouse, December 16, 2003.
- [33] L. Zhang and D. Manocha, *An efficient retraction-based RRT planner*. IEEE International Conference on Robotics and Automation, PP. 3743-3750, 2008.
- [34] J. Lee, O.S. Kwon, L. Zhang, and S.E. Yoon, *A selective retraction-based RRT planner for various environments*, IEEE Transactions on Robotics, Vol. 30, No. 4, PP. 1002-1011, 2011.
- [35] J. Pan, L. Zhang, and D. Manocha, *Retraction-based RRT planner for articulated models*, IEEE International Conference on Robotics and Automation, PP. 2529-2536, 2010.